Electron Energy Spectra from Intense Laser Double Ionization of Helium

R. Lafon,[1] J. L. Chaloupka,[1] B. Sheehy,[1] P. M. Paul,[2] P. Agostini,[2] K. C. Kulander,[3] and L. F. DiMauro[1]

[1]*Chemistry Department, Brookhaven National Laboratory, Upton, New York 11973*
[2]*SPAM, Centre d'Etudes de Saclay, 91191 Gif Sur Yvette, France*
[3]*TAMP, Lawrence Livermore National Laboratory, Livermore, California 94551*

(Received 16 November 2000)

The double ionization of helium in the strong-field limit has been studied using an electron-ion coincidence technique. The observed double ionization electron energy spectra differ significantly from the single ionization distributions. This gives new support to the rescattering model of double ionization and explicitly reveals the role of backward electron emission following the e-2e ionizing collision.

DOI: 10.1103/PhysRevLett.86.2762 PACS numbers: 32.80.Fb, 31.90.+s, 32.80.Rm

A neutral atom interacting with a sufficiently strong laser field will ionize even for photon energies well below the ionization threshold. For large photon numbers, the ionization process is best described as the suppression of the atomic Coulomb barrier by the laser field, which allows an electron to tunnel into the continuum. As the laser intensity is increased, the suppression of the barrier will become greater, and more tightly bound electrons may become liberated. This sequential ionization is most easily explained by the single active electron (SAE) approach, where only the outermost electron in the atom is affected by the laser field. Each electron effectively "waits" for the proper intensity before being liberated, without regard for the effects of the other electrons. This simple picture results in excellent agreement with the experimental single ionization yields, but it is not sufficient to describe the more complex double ionization observed in the laboratory [1,2]. This behavior is exemplified in Fig. 1 as a plot of the intensity dependent single and double ionization yields of helium. At intensities below 1 PW/cm^2, where the creation of He^{2+} via sequential ionization of the He^+ ground state is expected to be very small, there is an observed enhancement of the double ion yield of at least several orders of magnitude (shaded region). This nonsequential double ionization (NSDI) has been shown [1] to result from a direct two-electron ejection from the neutral helium ground state, and cannot be explained with an SAE model. NSDI has been observed in many of the noble gases [2,3], but has been most extensively studied in helium [1,4,5].

Mechanisms such as simple rescattering [6], rescattering with Coulomb refocusing and multiple returns [7], shakeoff [8], and collective tunneling [9] have been proposed. The electron-electron interaction has been included either as a time-dependent potential correction to the SAE approximation [10] or through the correlated energy sharing method [11,12], while numerical solutions of the Schrödinger equation for a 1D model [13] and 3D helium [14] are in progress. Moreover, signatures of the direct channel in the photoelectron energy spectrum have been found in two-photon double ionization [15]. Unfortunately, there has been a limited number of experimental results for suitable comparison to these theories.

Very recently, ion-recoil experiments in helium [5], neon [3], and electron-ion coincidence measurements in argon [16] and xenon [17] have provided new insights into the NSDI process. Both of the ion-recoil measurements [3,5] have been consistent with the rescattering model. The coincidence measurements in argon [16] showed that the momenta of the two outgoing electrons were correlated and that the distributions were compatible with the release of two electrons through rescattering with zero initial velocity. In the xenon study [17], the distribution of electrons detected in coincidence with Xe^{2+} appeared to be "hotter." Until now, the measurement of the double ionization electron spectra in helium has been hindered by experimental difficulties.

In this Letter, we present the first energy spectra of electrons liberated by the strong-field double ionization of helium that were detected in coincidence with the parent ions. Helium is the paradigm for strong-field investigations because of its simple two-electron structure, which allows for broader theoretical treatment versus more complex atoms. Also, as a consequence of its large binding energy, the laser intensity needed to ionize helium places it within the quasistatic limit of tunnel ionization. The latter point has been confirmed by numerous experimental [1,4,5,8,18] and theoretical [10,11,13–15] studies, resulting in a very comprehensive understanding of the single

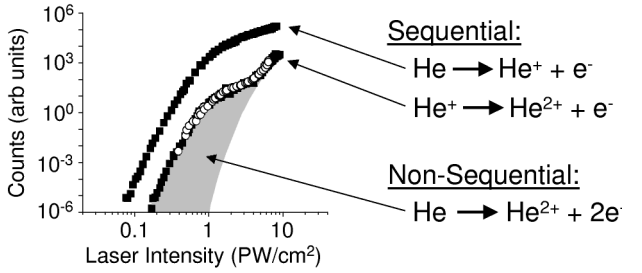

FIG. 1. The single and double ionization yields of ^{4}He (solid squares) as a function of laser intensity. Double ionization yields of ^{3}He (open circles) show clear agreement. The region of double ionization enhancement over the sequential tunneling prediction is shown shaded.

 0031-9007/01/86(13)/2762(4)$15.00

electron dynamics. However, the two-electron process has remained unclear. In our experiment, the electron distributions correlated to double ionization were examined at two intensities with 0.78-μm, 100-fs pulses. The electrons detected in coincidence with a doubly ionized helium atom show a remarkable enhancement at high energies compared to the electrons involved in the single ionization process. We will show that this implies rescattering in the backward direction.

The measurement of the two-electron energy distribution in helium has been plagued by two significant experimental issues. The first and most obvious is the miniscule rate of double as compared to single ionization. In Fig. 1, the single and double ionization yields of helium are shown as a function of intensity. The ratio of double to single ionization in the nonsequential region (shown shaded) is never larger than 1:500, making a coincidence measurement necessary to extract the greatly outnumbered double ionization electrons. The second difficulty arises from the high intensity needed to ionize helium. Since background ionization occurs over a much larger effective focal volume, even a small amount of contamination in the vacuum chamber can result in a significant number of ionization events. This places great demands on the target chamber base pressure and the purity of the target gas.

In order to generate an electron distribution that correlates to a specific ion species and charge state, an ion mass-to-charge spectrum must be recorded simultaneously with an electron time-of-flight spectrum. By detecting only one ion and one or more electrons in coincidence, it can be determined with some level of certainty that the detected ion and electrons were involved in the same ionization process. This level of certainty manifests itself in the number of "true" counts that are accumulated (the electrons and ion are positively correlated) versus the number of "false" or accidental counts (the electrons and ions are not correlated) [19]. The resulting true:false ratio can be calculated and used in the interpretation of the data.

The laser used in this study was a titanium:sapphire chirped-pulse amplification system utilizing a regenerative amplifier. It was operated at a repetition rate of 1–2 kHz and produced 0.78-μm, 100-fs pulses which were tightly focused to generate peak intensities as high as 10^{16} W/cm^2. The focal region was centered in a two-sided, pulsed-plate, electron-ion spectrometer. Electrons liberated in the ionization process were allowed to drift in a field-free region towards a microchannel plate (MCP) assembly. After a delay of 150 ns, an extraction voltage of -75 V was turned on to collect the ions. The delay was long enough to allow the majority of the liberated electrons to drift into the protected, field-free flight tube and short enough that the ion displacement due to thermal motion did not affect their efficient extraction towards the ion MCP. Both of these issues were verified in static-field and pulsed tests. The electron detector subtends a full angle of 10° and has an absolute collection and detection efficiency of roughly 1% and an energy resolution of 5%. Since the collection efficiency naturally depends on the angular distribution of the electrons, a typical value is quoted here. The ion detector has an absolute collection and detection efficiency of roughly 30% and a mass-to-charge resolution of 0.7%. The spectrometer sat within an ultrahigh vacuum chamber (10^{-10} torr), and the target gas was delivered via a leak valve into the entire chamber, while continually pumping with two turbomolecular pumps.

The spectrometer was first characterized with noncoincidence experiments. Previously studied electron spectra and ion ratio curves were reproduced in both static and pulsed modes. The coincidence scheme was then tested using a known gas mix of krypton and xenon. First, the "control" electron time-of-flight (TOF) spectra of pure krypton and pure xenon were recorded at an intensity of 4×10^{13} W/cm^2. Next, a coincidence measurement using the gas mix was performed at a Xe:Kr ion ratio of 8:1 and an overall xenon ion detection rate of 0.1/shot. The total, noncoincident electron and ion spectra from 65.9×10^6 laser shots were recorded, along with the ion and electron arrival times when only one ion was detected. With this information, it is straightforward to compile the coincident electron spectrum for any of the detected ions. Figure 2(a) shows the total electron TOF spectrum (solid line) generated with the gas mix, as well as the krypton spectrum (dashed line) generated with the pure gas. The kryptonlike features in the gas mix spectrum are hidden among the more abundant electrons from xenon. Figure 2(b) shows the krypton coincidence spectrum (solid line), which has been extracted from the total spectrum, and the pure krypton spectrum (dashed line). The improved agreement is unmistakable. The calculated true:false ratio was roughly 3:1. This test shows, in a clear and controlled fashion, the effectiveness of our coincidence technique.

Coincidence data using helium was taken at two intensities: the single ionization saturation intensity ($I_{\text{sat}} = 0.8$ PW/cm^2) and half of this value. Figure 3 shows the

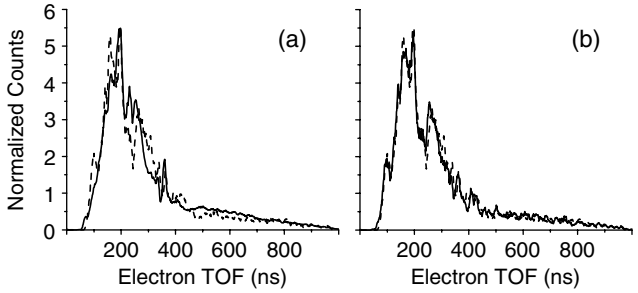

FIG. 2. The Xe/Kr gas mix test. In both plots, the dashed line is the pure krypton spectrum, while the solid line is (a) the total electron spectrum generated with the gas mix and (b) the krypton coincidence spectrum. All curves are normalized by their integrated values, smoothed from 1-ns to 10-ns resolution, and uncorrected for false counts.

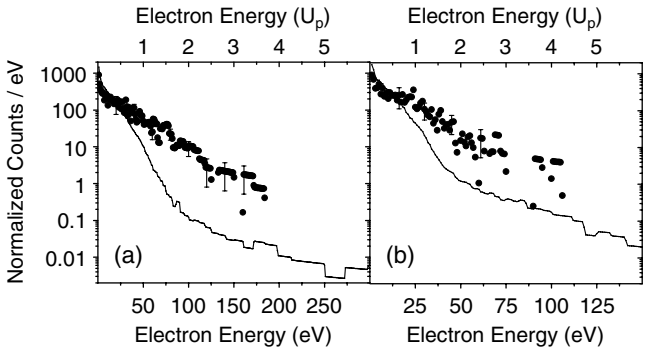

FIG. 3. The energy spectra for electrons detected in coincidence with $^3He^+$ (solid line) and $^3He^{2+}$ (circles) at (a) the single ionization saturation intensity (0.8 PW/cm^2) and (b) one-half of this value. Representative error bars for the double ionization electrons reflect the counting statistics and the true:false ratio. All curves are uncorrected for false counts. The ion ratio for double to single ionization is (a) 0.0013 and (b) 0.000 59.

energy spectra for electrons detected in coincidence with the single (solid line) and double ionization (circles) of ^{3}He. Helium-3 was used rather than ^{4}He to enhance the measurement sensitivity since the $^4He^{2+}$ and background H_2^+ ion peaks are difficult to differentiate. The curves are normalized by their integrated value, and the horizontal axes show the absolute electron energy as well as the energy scaled to the ponderomotive potential (U_p) at the peak laser intensity. U_p is the cycle-averaged quiver energy of an electron oscillating in the field and is linearly proportional to the intensity. Figure 3(a) shows the electron energy spectra measured at I_{sat}. A total of 205×10^6 laser shots were taken, yielding 1058 double ionization coincidences. The detection rate of $^3He^+$ was roughly one in five laser shots, and the rate of background ions was one in three. The ion ratio of double to single ionization was 0.0013. High count rates were used to improve the counting statistics on the double ionization electron spectrum, resulting in an overall true:false ratio of roughly 1:1. However, for the high-energy electrons, where the abundance of false electrons is very low, the true:false ratio is much greater. For example, at 100 eV, the effective true:false ratio is 100:1. This is simply due to the paucity of high-energy electrons that can contribute to accidental counts. As a result, correcting the double ionization spectrum by subtracting away false counts has very little effect on the electron distribution beyond 50 eV. Figure 3(b) shows the electron energy spectra generated at $I_{sat}/2$. A total of 190×10^6 laser shots were taken, yielding 450 double ionization coincidences. The detection rate of $^3He^+$ was roughly one in four laser shots, and the rate of background ions was one in five. The ion ratio of double to single ionization was 0.000 59. Again, the overall true:false ratio was calculated to be roughly 1:1, but, as before, the effective ratio at high energies is much higher.

The double ionization electron spectra in Fig. 3 are significantly different from those resulting from single ionization. The single ionization features can be easily understood using a simple quasiclassical model of the ionization dynamics [4,6,18]. Electrons are promoted into the continuum at rest at all phases of the field, with a probability given by the instantaneous dc-tunneling rate. Their subsequent evolution is approximated from the classical equations of motion, with the velocity having two components: a quiver motion from the oscillating laser field and a drift velocity. In a short pulse, the measured final velocity is determined solely by the phase of the field at which the electron is set free [6]. An electron released at the peak of the field will gain zero drift energy, while an electron released at the null of the field will gain $2U_p$. Since the maximum of the tunneling rate coincides with the peak of the laser field, the single ionization electron distribution exhibits a peak at zero energy with a sharp drop towards $2U_p$. The long plateau extending to $10U_p$ is due to electrons that are born after the peak of the field that return to the core where they backscatter elastically. Backward scattering is much more effective for producing high final kinetic energies since the electron velocity and the laser field have opposite signs, leading to further acceleration.

In contrast, the double ionization spectra of Fig. 3 show a much slower rate of decrease with energy, extending at least to $4U_p$ at both laser intensities. The rescattering model [6] can also explain this higher energy distribution. When the first electron returns to the core with a kinetic energy larger than the binding energy of the second electron, it can liberate the second electron, giving rise to two electrons that share the excess energy. These e-$2e$ collisions take place near a minimum in the oscillating electric field of the laser and when the returning electrons are near their maximum velocities. The resultant lowering of the electron's kinetic energy via the inelastic process is equivalent to adding a large backward component to its drift velocity. Similarly, the ionized electron must have a low velocity relative to the quiver velocity at that phase of the field, resulting in its drift velocity also having a substantial backward component. Thus after the collision, it is the backscattered e-$2e$ electrons that end up with the largest final velocities. To illustrate this, a model calculation was performed that initiated electron trajectories via tunneling at all phases of the field, where those returning to the ion core could lead to an e-$2e$ ionizing collision. The following simplifying assumptions were made, guided by the observed e-$2e$ triply differential cross sections (TDCS) for hydrogen and helium [20–22]. The postcollision velocities were assumed to be along the polarization direction, with one parallel ("forward") and one antiparallel ("backward") to the velocity of the returning electron. Near threshold, the two electrons shared the excess energy equally. For higher collision energies (at approximately twice the threshold energy), the forward scattered electron was given 90% of the excess energy and the rest was given to the one scattered backward. Figure 4 shows

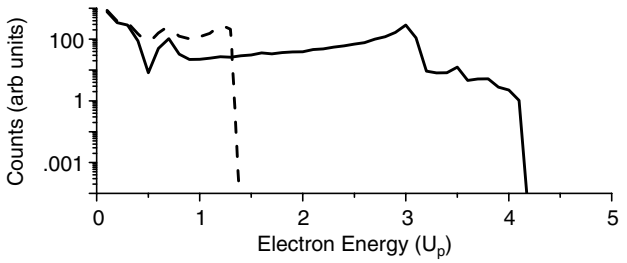

FIG. 4. Calculated electron energy spectra of the NSDI of helium via rescattering with the full calculation (solid line) and with only forward initial velocities (dashed line). In both cases, the results are spatially and temporally averaged over the laser pulse.

the calculated electron energy spectra at an intensity of 0.8 PW/cm^2. The spectrum from the full calculation (solid line) extends beyond $4U_p$, while the result obtained when both electrons were initially scattered into the forward direction (dashed line) cuts off well before $2U_p$. Clearly, the electrons with energies larger than $2U_p$ must be the result of an initial backward velocity. Essentially the same results are obtained at the other experimental intensity of 0.4 PW/cm^2. The structures appearing in the distributions are artifacts of the calculation due to the discrete partitioning of the excess collision energy and the restricted angular distribution of the scattering directions. Relaxing these constraints will remove the structure, but will not affect the overall shape. The distributions are not very sensitive to reasonable variations of the scattering momentum distributions. The important feature, namely the extension to energies greater than $2U_p$, is always present when backscattering is included. It should be noted that the rescattering model in general favors final drifts of both electrons along the same (backward) direction. Even in the case of antiparallel *initial* velocities, the *final* drift velocities tend to align. This is compatible with observations in argon [16]; however, their observed electron distributions were found to be peaked at the same nonzero energy for both electrons. Our observations in helium show no such unique conditions. Rather, a broader distribution is observed, with forward scattering contributing for energies lower than $2U_p$, and backward scattering contributing out to $4U_p$. This discrepancy may be a result of the additional electrons in the more complex argon atom leading to different double ionization dynamics.

In conclusion, our helium electron-ion coincidence measurements are in general qualitative agreement with other recent experiments [3,5,16,17] in that they are compatible with the rescattering mechanism of NSDI. Our results also provide new information about the maximum energy of the photoelectrons produced in the strong-field NSDI of helium. In particular, this serves to emphasize the role of backward electron emission following the e-$2e$ ionizing collision. It is expected that this work will stimulate full quantum calculations of the two-electron energy distribution.

The experiments were carried out at Brookhaven National Laboratory under Contract No. DE-AC02-98CH10886 with the U.S. Department of Energy and supported by its Division of Chemical Sciences, Office of Basic Energy Sciences, and in part under the auspices of the U.S. Department of Energy at the Lawrence Livermore National Laboratory under Contract No. W-7405-ENG-48. R. L., L. F. D., P. M. P., and P. A. acknowledge travel support from NATO under Contract No. SA.5-2-05(RG910678).

[1] B. Walker *et al.,* Phys. Rev. Lett. **73**, 1227 (1994).
[2] S. Larochelle, A. Tablepour, and S. L. Chin, J. Phys. B **31**, 1201 (1998).
[3] R. Moshammer *et al.,* Phys. Rev. Lett. **84**, 447 (2000).
[4] B. Sheehy *et al.,* Phys. Rev. A **58**, 3942 (1998).
[5] Th. Weber *et al.,* Phys. Rev. Lett. **84**, 443 (2000).
[6] P. B. Corkum, Phys. Rev. Lett. **71**, 1994 (1993).
[7] G. L. Yudin and M. Ivanov, Phys. Rev. A **63**, 033404 (2001).
[8] D. N. Fittinghoff *et al.,* Phys. Rev. Lett. **69**, 2642 (1992).
[9] U. Eichmann *et al.,* Phys. Rev. Lett. **84**, 3550 (2000).
[10] J. B. Watson *et al.,* Phys. Rev. Lett. **78**, 1884 (1997).
[11] A. Becker and F. H. M. Faisal, Phys. Rev. A **59**, R1742 (1999).
[12] A. Becker and F. H. M. Faisal, Phys. Rev. Lett. **84**, 3546 (2000).
[13] R. Panfili *et al.,* in *Multiphoton Processes,* edited by L. F. DiMauro, R. R. Freeman, and K. C. Kulander (AIP, New York, 2000), p. 265; M. Lein, E. K. U. Gross, and V. Engel, Phys. Rev. Lett. **85**, 4707 (2000).
[14] K. T. Taylor *et al.,* Laser Phys. **9**, 98 (1999).
[15] M. A. Kornberg and P. Lambropoulos, J. Phys. B **32**, L603 (1999).
[16] Th. Weber *et al.,* Nature (London) **405**, 658 (2000).
[17] B. Witzel, N. A. Papadogiannis, and D. Charalambidis, Phys. Rev. Lett. **85**, 2268 (2000).
[18] B. Walker *et al.,* Phys. Rev. Lett. **77**, 5031 (1996).
[19] V. Stert *et al.,* Eur. Phys. J. D **5**, 97 (1999).
[20] J. Röder *et al.,* J. Phys. B **30**, 1309 (1997); J. Röder *et al.,* Phys. Rev. Lett. **79**, 1666 (1997).
[21] S. Rioual *et al.,* J. Phys. B **31**, 3117 (1998).
[22] I. Bray, Aust. J. Phys. **53**, 355 (2000).